



Article

Influence of Ethanol Parametrization on Diffusion Coefficients Using OPLS-AA Force Field

Bruno Zêzere ¹, Tiago V. B. Fonseca ¹, Inês Portugal ¹, Mário M. Q. Simões ², Carlos M. Silva ^{1,*}
and José R. B. Gomes ^{1,*}

¹ CICECO—Aveiro Institute of Materials, Department of Chemistry, University of Aveiro, Campus Universitário de Santiago, 3810-193 Aveiro, Portugal

² LAQV-REQUIMTE, Department of Chemistry, University of Aveiro, Campus Universitário de Santiago, 3810-193 Aveiro, Portugal

* Correspondence: carlos.manuel@ua.pt (C.M.S.); jrgomes@ua.pt (J.R.B.G.)

Abstract: Molecular dynamics simulations employing the all-atom optimized potential for liquid simulations (OPLS-AA) force field were performed for determining self-diffusion coefficients (D_{11}) of ethanol and tracer diffusion coefficients (D_{12}) of solutes in ethanol at several temperature and pressure conditions. For simulations employing the original OPLS-AA diameter of ethanol's oxygen atom (σ_{OH}), calculated and experimental diffusivities of protic solutes differed by more than 25%. To correct this behavior, the σ_{OH} was reoptimized using the experimental D_{12} of quercetin and of gallic acid in liquid ethanol as benchmarks. A substantial improvement of the calculated diffusivities was found by changing σ_{OH} from its original value (0.312 nm) to 0.306 nm, with average absolute relative deviations (AARD) of 3.71% and 4.59% for quercetin and gallic acid, respectively. The new σ_{OH} value was further tested by computing D_{12} of ibuprofen and butan-1-ol in liquid ethanol with AARDs of 1.55% and 4.81%, respectively. A significant improvement was also obtained for the D_{11} of ethanol with AARD = 3.51%. It was also demonstrated that in the case of diffusion coefficients of non-polar solutes in ethanol, the original $\sigma_{OH} = 0.312$ nm should be used for better agreement with experiment. If equilibrium properties such as enthalpy of vaporization and density are estimated, the original diameter should be once again adopted.

Keywords: diffusion coefficient; liquid ethanol; molecular dynamics simulations; OPLS-AA



Citation: Zêzere, B.; Fonseca, T.V.B.; Portugal, I.; Simões, M.M.Q.; Silva, C.M.; Gomes, J.R.B. Influence of Ethanol Parametrization on Diffusion Coefficients Using OPLS-AA Force Field. *Int. J. Mol. Sci.* **2023**, *24*, 7316. <https://doi.org/10.3390/ijms24087316>

Academic Editor: Majdi Hochlaf

Received: 16 February 2023

Revised: 3 April 2023

Accepted: 8 April 2023

Published: 15 April 2023



Copyright: © 2023 by the authors. Licensee MDPI, Basel, Switzerland. This article is an open access article distributed under the terms and conditions of the Creative Commons Attribution (CC BY) license (<https://creativecommons.org/licenses/by/4.0/>).

1. Introduction

Tracer binary diffusion coefficients (D_{12}) are essential when designing equipment or optimizing production, both for conventional and newly developed rate-controlled processes [1,2]. Even though large databases of diffusion coefficients have been published [3], a lack of data is still verified, especially for bioactive polar solutes in polar dense solvents such as ethanol.

The predominant method for experimental determination of D_{12} values is the Taylor dispersion or Chromatographic Peak-Broadening method [4–10], which is time-consuming and requires specialized equipment and expensive solute standards. Alternatively, one may recur to phenomenological models such as the widely known Wilke–Chang equation [11,12]. However, for polar-solvent systems, the results achieved by such purely predictive equations are often moderate [3,13] since these models do not account for strong interactions between the molecules, for example hydrogen bonds. Data-correlative models, such as the 2-parameter equations of Dymond–Hildebrand–Batschinski (DHB) [14–16] and the Rice and Gray-based approach by Zêzere et al. [3], tend to yield better results, but their big disadvantage is the need of experimental data to determine the optimized parameters for each system.

An alternative approach for predicting D_{12} considers Machine Learning (ML) algorithms as, for instance, the model proposed by Aniceto et al. [13] for polar-solvent systems.

Although low deviations were achieved (average deviations of 5.07%), this approach has yet to withstand the test of time since most of these algorithms work as a “black box”, being hard to anticipate the magnitude of the deviations for a given system. Nevertheless, this is currently the best option for a “quick and dirty” estimation of D_{12} of a polar-solvent system and should not be disregarded. ML models have also been developed for the D_{12} prediction of non-polar systems [13] and of different solutes in supercritical CO₂ [17].

Other approaches include Artificial Neural Networks (ANN) and Molecular Dynamics (MD) simulations. ANN have been employed for the prediction of self-diffusion coefficients (D_{11}) in pure liquids [18] and in binary fluid mixtures [19], whereas MD simulations have been successfully used, e.g., for the estimation of D_{12} , both in liquids [20] and in supercritical fluids [21], and of D_{11} in liquids [22,23].

MD has been used to simulate the dynamics of molecular systems within a given period of time, by numerically integrating Newton’s equations of motion and upon consideration of quantum or classical mechanics to calculate the forces between the particles in the molecular systems under study, leading to the so-called *ab initio* MD (AIMD) or classical MD approaches, respectively, with the former being much more time consuming than the latter [24]. Classical MD simulations rely on sets of empirical parameters, a.k.a. force fields, to calculate the intramolecular and intermolecular interactions between the constituting particles in a specific system. Different degrees of empiricism originate different force fields, and different parametrizations define the limits of their application. There has been a continuous effort to develop new, or improve existing, force fields, which can be (i) coarse-grained, such as MARTINI [25], where groups of several atoms are represented by a single bead; (ii) united-atom, such as United-Atom Transferable Potential for Phase Equilibria (TraPPE-UA) [26], where, for example, hydrogen containing moieties as CH, CH₂, and CH₃ groups are treated as single unified interaction centers with masses corresponding to the sum of the masses of C and H atoms in the CH_x group; and (iii) all-atom, such as the General AMBER Force Field (GAFF) [27] and the All-Atom Optimized Potential for Liquid Simulations (OPLS-AA) [28], where all atoms are represented individually. The force fields are under continuous improvement, and new versions are published on a regular basis. For example, OPLS-AA has been the cornerstone of other force fields, e.g., L-OPLS-AA [29,30], OPLS-AA/M [31], and OPLS4 [32], which were introduced to overcome some limitations of the original set of parameters. The L-OPLS-AA enabled a more accurate reproduction of liquid properties of long alkanes, alcohols, esters, and glyceryl monooleate that was not possible using the OPLS-AA [29,30]; the OPLS-AA/M improved on previous iterations of the OPLS-AA force fields regarding its ability to reproduce both gas-phase conformer energies for longer peptides and aqueous phase experimental properties [31]; in OPLS4, the new parameters allowed for more accurately predicting protein–ligand binding affinities by addressing limitations in the representation of molecular ions, sulfides, and aryl sulfur and a general improvement in model hydration [32]. Consequently, the accuracy and the precision of the simulations tend to improve with time, which combined with the reducing costs of increasing computational power and efficient algorithms, make classical MD simulation an enticing approach for a D_{12} estimation that, in some cases, may even compete with experimental studies.

The main focus of this work was to assess (and refine) the performance of OPLS-AA [28] for the calculation of transport properties, namely, D_{12} of specific solutes in liquid ethanol and D_{11} of ethanol. OPLS-AA was chosen due to its good description of liquid organic systems [33], the vast number of parameters available, compatibility, and easiness of implementation. Furthermore, some authors have shown that OPLS-AA can provide good results for D_{12} , for example Zézere et al. [20], who estimated D_{12} of ketones and aldehydes in pressurized liquid ethanol and by Vaz et al. [21], who estimated D_{12} of ketones in SC-CO₂. However, have regard for the computation of D_{12} of protic solutes in ethanol and D_{11} of ethanol [34], as these properties tend to be overestimated when using OPLS-AA, as will be presented further in this work. At this point, it is important to stress that the determination of accurate D_{12} of protic solutes in liquid ethanol is of utmost importance to

design and optimize industrial equipment and kinetic processes. Despite some correlations available in the literature [14–16], including some originating in our group [3], the fact is that there is no general theory to accurately estimate D_{12} of polar systems without having experimental (or accurate computational) data. Therefore, new approaches for determining such values are expected to have an impact on the field.

Several modifications to OPLS-AA have been published to improve D_{11} calculations of ethanol and other alcohols. For instance, Kulschewski and Pleiss [34] proposed the adjustment of the hydroxyl group partial charges to better describe D_{11} of alcohols, but this parametrization still originated significant differences (e.g., for ethanol, the estimation of D_{11} differs up to 22%, depending on the experimental value used for comparison). Another very recent work by Zhang et al. [35] focusing on C1 to C10 primary alcohols considered a combination of L-OPLS parameters for the hydrocarbon tail and OPLS-AA parameters for the hydroxyl group, as suggested by Zangi [33], with additional tiny adjustments (scale factors in the range of 1.00–1.03) of the partial charges. This approach, the so-called mixed-OPLS-AA model refinement of the OPLS-AA force field for liquid alcohols with scaled charges [34], decreased the deviations between experimental and estimated D_{11} to values in the range of -8% for nonan-1-ol and 5% for ethanol [35]. For comparison, the corresponding deviations calculated with the original mixed-OPLS-AA model [33] (i.e., without the charge scaling) were 19% and 34% , respectively. Other force fields, such as OPLS4 [32], extensively tested by Baba et al. [22] for the prediction of D_{11} over 152 diverse pure liquids at various temperatures, achieved maximum deviations roughly under 20% for ethanol. Petracic and Delhommelle [36] tested OPLS-UA (united atom version of OPLS-AA), which, similarly to OPLS-AA, overestimates D_{11} of ethanol by roughly 25% , on average, due to density underestimation (around -4%). Enforcing the experimental density of ethanol decreased the D_{11} value; the calculated value still slightly overestimates the experimental result, yet to a smaller extent [36]. Cardona et al. [37] tested both GAFF and TraPPE-UA for the estimation of D_{11} for ethanol, reporting deviations of -2.08% and 7.47% , respectively. Finally, Schnabel et al. [38] proposed an ethanol rigid anisotropic united-atom model, based on Lennard-Jones and Coulombic interactions, which achieved average deviations of -6% for D_{11} of liquid ethanol [39].

Not disregarding the previous proposed corrections and/or parameterizations, a different approach for refinement of OPLS-AA when computing either D_{12} or D_{11} is presented in this work. In particular, the influence of the diameter of ethanol's oxygen atom (σ_{OH}) on the diffusion coefficients of systems embodying hydrogen-bonding solvents is analyzed. This correction was triggered by Hirschfelder et al. [40], who claimed that the diameters of molecules tend to be smaller when computed from transport properties than when equilibrium properties are used. Here, we show that a reparameterization, i.e., smaller ethanol σ_{OH} value, can be successfully introduced in the case of self- and binary diffusion coefficients (transport properties) in opposition to equilibrium properties (namely, density and enthalpy of vaporization) for which the original parametrization affords better results. A database of experimental D_{11} and D_{12} values, together with the above-mentioned equilibrium data, was compiled in order to validate the MD simulations and assumptions.

2. Results and Discussion

2.1. D_{12} of Quercetin and Gallic Acid in Liquid Ethanol: Optimization of the Oxygen's Radius

MD simulations of diffusion coefficients of polar solutes containing OH groups in liquid ethanol consistently generate D_{12} with high deviations in relation to experimental data. For example, for quercetin in liquid ethanol at 1 bar modelled with the original OPLS-AA parameters, deviations of 26.61% and 31.78% were found at 303.15 K and 323.15 K, respectively. Similarly, for gallic acid at the same conditions, the deviations were 29.13% and 35.25% at 303.15 K and 333.15 K, respectively. Noteworthy, in both cases, the deviations increase with temperature, as previously reported for D_{12} calculations of ketones and aldehydes in liquid ethanol [20]. The deviations are also consistent with those from previous MD studies focusing on diffusivities of alcohols, as summarized in the Introduction section.

Hirschfelder et al. [40] stated that the diameters of molecules tend to be smaller when computed based on transport properties than when using equilibrium properties. Therefore, we decided to investigate the effects of changing the diameter of the oxygen atom from the ethanol hydroxyl group upon the D_{12} values derived from classical MD simulations. In the OPLS-AA force field, the diameter of the aliphatic alcohol oxygen atom (σ_{OH}) is 0.312 nm. Thus, we performed simulations of ethanolic solutions of quercetin and gallic acid at the conditions reported in Table 1, using σ_{OH} for ethanol in the range 0.304 to 0.312 nm and without changing the remaining simulation parameters (Figure 1 and Table S1). The best comparison of calculated and experimental D_{12} of quercetin and gallic acid in ethanol (Table 1) was obtained when using $\sigma_{OH} = 0.306$ nm. Encouragingly, the optimum diameter found is close to the 0.307 nm utilized in the OPLS-UA force field [28]. In practice, this change implies that the molecules of ethanol become closer to each other than in the original parametrization; hence, density increases (as it will be shown further) and the free volume of the solvent decreases, lowering the D_{12} values. In the case of quercetin, at the simulated conditions of 303.15 K and 1 bar, 303.15 K and 150 bar, 323.15 K and 1 bar, and 323.15 K and 150 bar, the newly found deviations ranged between -6.30% and 4.22% (individual results are given in Table 1), with global average relative deviations (ARD, defined in Section 3.1) and average absolute relative deviations (AARD, defined in Section 3.1) of -0.04% and 3.71% , respectively. This is a massive improvement over the results achieved with the initial value $\sigma_{OH} = 0.312$ nm. A similar improvement was confirmed for gallic acid with the new σ_{OH} value giving relative deviations (RD, defined in Section 3.1) between -5.31% and 6.08% and ARD and AARD values of 1.05% and 4.59% , respectively. Although the ARD value is close to zero, for both solutes, a strong dependence between RD and T is verified with the D_{12} values being slightly underestimated at 303.15 K and overestimated at 323.15 K and 333.15 K, as can be seen in Table 1.

Table 1. Experimental (D_{12}^{exp}) and computed (D_{12}^{MD}) diffusion coefficients of quercetin and gallic acid in liquid ethanol at various temperatures and pressures. The computer simulations used $\sigma_{OH} = 0.306$ nm for ethanol, and the calculated diffusivities were evaluated in comparison with experimental data in terms of the relative deviation (RD), average relative deviation (ARD), and average absolute relative deviation (AARD).

Solute	T (K)	P (bar)	$D_{12}^{\text{exp}} \pm \Delta D_{12}^{\text{exp}}$ ($10^{-9} \text{ m}^2 \text{ s}^{-1}$)	$D_{12}^{\text{MD}} \pm \Delta D_{12}^{\text{MD}}$ ($10^{-9} \text{ m}^2 \text{ s}^{-1}$)	RD (%)
Quercetin	303.15	1	0.459 ± 0.003	0.430 ± 0.014	-6.30
	303.15	150	0.414 ± 0.002	0.409 ± 0.010	-1.21
	323.15	1	0.681 ± 0.002	0.702 ± 0.003	3.13
	323.15	150	0.616 ± 0.003	0.642 ± 0.036	4.22
					ARD = -0.04% AARD = 3.71%
Gallic acid	303.15	1	0.508 ± 0.009	0.481 ± 0.014	-5.31
	323.15	1	0.758 ± 0.006	0.776 ± 0.028	2.37
	333.15	1	0.905 ± 0.011	0.960 ± 0.028	6.08
					ARD = 1.05% AARD = 4.59%

The expected dependency of D_{12} with T , P , and Stokes–Einstein abscissae (T/μ_1) was generally conserved, as can be observed in Table 1 and in Figure 2. D_{12} increases with rising temperature due to the higher internal energy and higher free volume of the system, which facilitate diffusion. Raising the pressure decreases the free volume of the solvent and increases the energy required for the solute to escape from the force field generated by the solvent, thus penalizing its diffusion [41–43]. As for the Stokes–Einstein abscissae, a linear relation between D_{12} and T/μ_1 was found in both cases, with R^2 values of 0.9737 and 1.000 for quercetin and gallic acid, respectively.

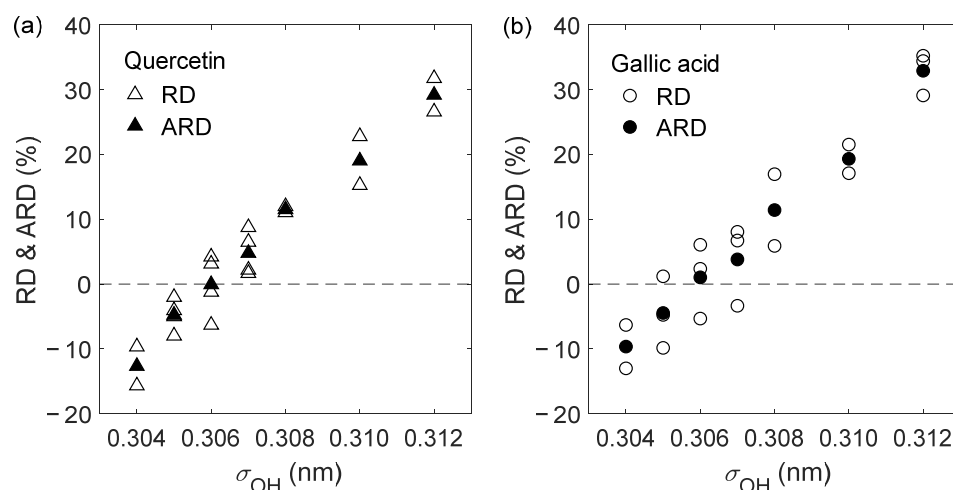


Figure 1. Relative deviations (RD) of D_{12} of (a) quercetin (triangles) and of (b) gallic acid (circles) in liquid ethanol versus ethanol's oxygen diameter (σ_{OH}). Empty symbols are individual RD values at different T and P conditions, while filled symbols are average relative deviations computed from the RD values obtained at each condition.

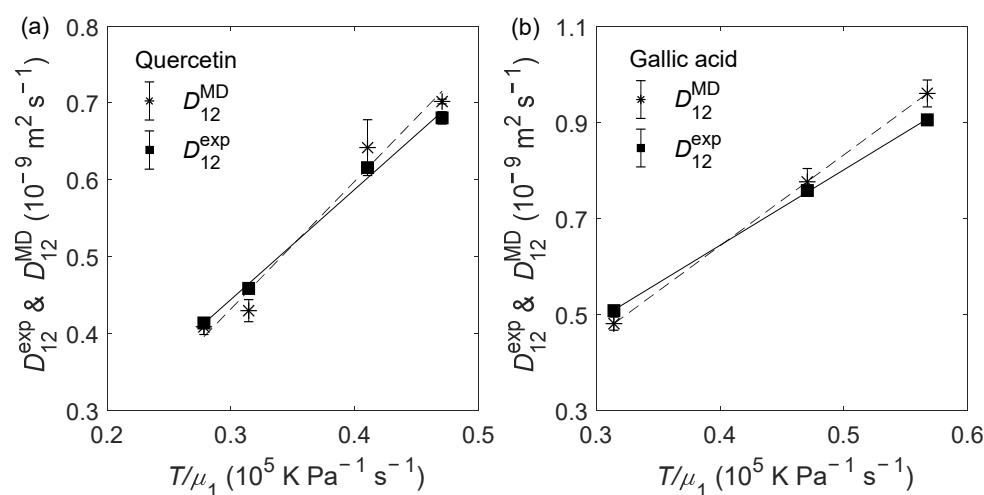


Figure 2. Experimental (D_{12}^{exp} , ■) and computed (D_{12}^{MD} , *) diffusion coefficients in liquid ethanol versus Stokes–Einstein abscissae (T/μ_1): (a) quercetin, and (b) gallic acid. The viscosity values were estimated by the Mamedov equation, as proposed by Cano-Gómez et al. [44].

2.2. D_{12} of Organic Solutes in Liquid Ethanol: Oxygen's Radius Validation and Cases of Applicability

For validation of the new proposed parametrization, we selected two OH-bearing systems with polar ends, namely, ibuprofen, an organic acid, and butan-1-ol, a primary alcohol, both in liquid ethanol. Alternative compounds for testing would be phenol and benzoic acid, but, unfortunately, the experimental diffusivities for these two compounds are scarce. As with the previous two systems, when employing ethanol's $\sigma_{OH} = 0.312$ nm, the D_{12} values deviate up to 32.24% from the experimental value for ibuprofen and up to 33.20% for butan-1-ol at the tested conditions (see Table S2 for detailed results). When using $\sigma_{OH} = 0.306$ nm, the maximum deviation decreased to 4.26% and 8.86% for ibuprofen and butan-1-ol, respectively, with AARD = 1.55% and ARD = 0.70% for ibuprofen and AARD = 4.81% and ARD = 4.05% for butan-1-ol, confirming the improvements introduced by the proposed parameterization, as observed for the previous two systems. Furthermore, the dependency with T and P was also conserved, as can be evidenced by the results in Table 2. As for the Stokes–Einstein relation, depicted in Figure 3, once again, a linear

relation was found between D_{12}^{MD} and T/μ_1 with $R^2 = 0.9781$ (experimental $R^2 = 0.9891$) for ibuprofen and for butan-1-ol, for which only two points were computed.

Table 2. Experimental (D_{12}^{exp}) and computed (D_{12}^{MD}) diffusion coefficients of ibuprofen and butan-1-ol in liquid ethanol at various temperatures and pressures. The computer simulations used $\sigma_{\text{OH}} = 0.306$ nm for ethanol, and the calculated diffusivities were evaluated in comparison with experimental data in terms of the relative deviation (RD), average relative deviation (ARD), and average absolute relative deviation (AARD).

Solute	T (K)	P (bar)	$D_{12}^{\text{exp}} \pm \Delta D_{12}^{\text{exp}}$ ($10^{-9} \text{ m}^2 \text{ s}^{-1}$)	$D_{12}^{\text{MD}} \pm \Delta D_{12}^{\text{MD}}$ ($10^{-9} \text{ m}^2 \text{ s}^{-1}$)	RD (%)
ibuprofen	298.15	100	0.518 ± 0.070	0.528 ± 0.011	1.93
	308.15	1	0.693 ± 0.070	0.686 ± 0.023	−1.01
	308.15	300	0.581 ± 0.070	0.567 ± 0.007	−2.41
	323.15	1	0.928 ± 0.070	0.936 ± 0.020	0.86
	323.15	300	0.754 ± 0.070	0.754 ± 0.018	0.00
	333.15	100	1.04 ± 0.07	1.04 ± 0.02	0.10
	333.15	200	0.986 ± 0.070	1.03 ± 0.03	4.26
	333.15	300	0.910 ± 0.070	0.927 ± 0.011	1.87
					ARD = 0.70%
					AARD = 1.55%
butan-1-ol	298.15	1	0.927	0.920 ± 0.011	−0.76
	333.15	1	1.84	2.00 ± 0.06	8.86
					ARD = 4.05%
					AARD = 4.81%

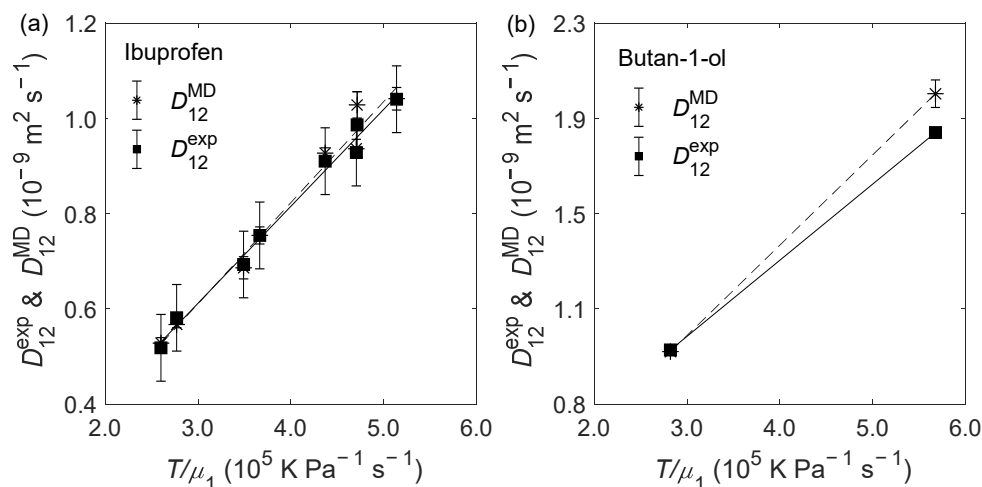


Figure 3. Experimental (D_{12}^{exp} , ■) and computed (D_{12}^{MD} , *) diffusion coefficients in liquid ethanol versus Stokes–Einstein abscissae (T/μ_1) for (a) ibuprofen and (b) butan-1-ol. The viscosity values were estimated by the Mamedov equation, as proposed by Cano-Gómez et al. [44].

So far, the new parametrization improvements are independent of the actual functional group of the solute, i.e., alcohol (OH) or organic acid (COOH), confirming the results for quercetin (with five OH groups) and gallic acid (with three OH groups and one COOH group). To further study the validity of this hypothesis, additional simulations were performed for compounds without the OH moiety, namely, two hydrogen-bond-acceptor solutes (propanone and butanal) and two non-polar solutes (propane and benzene).

The D_{12}^{MD} values of propanone and butanal were computed in previous work [20], where the σ_{OH} value of 0.312 nm yielded satisfactory results, with AARD values between 9.48% and 12.18% and ARD between 8.37% and 12.18% for the ketones studied. For aldehydes, the situation was similar, with AARD between 6.30% and 9.11% and ARD

between 1.00% and 5.67%. All the simulations were carried out at temperatures between 303.15 K and 333.15 K and pressures up to 150 bar [20]. In this work, to test the new proposed σ_{OH} value, two different temperatures (303.15 K and 333.15 K) and one value of pressure (1 bar) were simulated, for both solutes, using the computational procedure reported by Zêzere et al. [20], this time with 3 ns of equilibrium and 3 ns of production. Only one value of pressure was simulated since no strong dependence between P and RD has been found, either in Ref. [20] or in the present study. For propanone, at 303.15 K, the newly computed D_{12}^{MD} value shows higher absolute deviation (RD = -17.63%) than the one computed with $\sigma_{\text{OH}} = 0.312$ nm, for which RD = 1.55% . However, at 333.15 K, the situation is quite the opposite, with the newly computed D_{12}^{MD} value achieving a lower absolute RD value (RD = 2.08%) than the one achieved with $\sigma_{\text{OH}} = 0.312$ nm (RD = 23.53%). In this particular case, while the absolute RD value at higher T is lower, when setting $\sigma_{\text{OH}} = 0.306$ nm, it comes at a cost of degraded performance at lower T , i.e., 303.15 K. The same behavior is verified for the aldehyde (butanal), for which the value of RD increases (from -5.15% to -24.48%) at 303.15 K and 1 bar and decreases (from 16.94% to -0.07%) at 333.15 K and 1 bar. Hence, for propanone and butanal, additional corrections are needed to translate the experimental dependence of the diffusivities with temperature, which affects also the data calculated with the ethanol's σ_{OH} value of 0.312 nm [20].

As for the non-polar solutes (benzene and propane), the D_{12}^{MD} values obtained with $\sigma_{\text{OH}} = 0.306$ nm present larger deviations in relation to D_{12}^{exp} than when the $\sigma_{\text{OH}} = 0.312$ nm value is used. For benzene, at 313.15 K and 1 bar, $D_{12}^{\text{MD}} = 2.28 \times 10^{-9} \pm 0.08 \times 10^{-9} \text{ m}^2 \text{ s}^{-1}$ when considering $\sigma_{\text{OH}} = 0.312$ nm and $D_{12}^{\text{MD}} = 1.85 \times 10^{-9} \pm 0.02 \times 10^{-9} \text{ m}^2 \text{ s}^{-1}$ when considering $\sigma_{\text{OH}} = 0.306$ nm, which correspond to RD of 0.00% and -18.86% , respectively. As for propane, the simulations at 323.15 K and 103 bar achieved similar results with $D_{12}^{\text{MD}} = 3.10 \times 10^{-9} \pm 0.05 \times 10^{-9} \text{ m}^2 \text{ s}^{-1}$ with $\sigma_{\text{OH}} = 0.312$ nm and $D_{12}^{\text{MD}} = 2.55 \times 10^{-9} \pm 0.08 \times 10^{-9} \text{ m}^2 \text{ s}^{-1}$ when $\sigma_{\text{OH}} = 0.306$ nm, corresponding to RD values of 3.68% and -14.72% , respectively.

To conclude this section, it is now safe to assume that the optimal σ_{OH} value is tied to the solute containing OH, or not, independently of the functional group where the atoms are. Considering the studied cases, when the solute is protic (i.e., the solute can participate in hydrogen bonds as donor and as acceptor), best results are obtained when σ_{OH} takes the value of 0.306 nm for the D_{12} calculation. Conversely, when the solute is non-polar, the value for σ_{OH} should be 0.312 nm. In the case of solutes with the ability to be hydrogen bond acceptors but not hydrogen bond donors, e.g., ketones and aldehydes, the preferred σ_{OH} should be 0.312 nm since any lower value would cause RD to increase at lower T , despite decreasing RD at higher T values.

2.3. D_{11} of Liquid Ethanol

The influence of the σ_{OH} parameter was further tested on the computation of D_{11} of liquid ethanol at 1 bar and at T between 298.15 K and 333.15 K. When parametrizing ethanol with $\sigma_{\text{OH}} = 0.312$ nm, the achieved RD values were between 24.05% and 35.38% , with AARD = 30.62% and ARD = 30.62% (see Table S3 for more details). However, and similarly to the results for protic solutes, when parametrizing ethanol with $\sigma_{\text{OH}} = 0.306$ nm, the achieved results drastically improve with the new-found RD between -5.91% and -0.77% , AARD = -3.51% , and ARD of the same value, as reported in Table 3. Furthermore, and similarly to what was verified for the D_{12} calculation, the computed D_{11} of ethanol follows the expected trends (i.e., increasing with T and the Stokes–Einstein coordinates). As depicted in Figure 4, there is a linear relation between D_{11} and T/μ_1 with $R^2 = 0.9997$ (experimental value of 0.9958).

Table 3. Experimental (D_{11}^{exp}) and computed (D_{11}^{MD}) self-diffusion coefficient of ethanol. The computer simulations used $\sigma_{\text{OH}} = 0.306$ nm for ethanol, and the calculated diffusivities were evaluated in comparison with experimental data in terms of the relative deviation (RD), average relative deviation (ARD), and average absolute relative deviation (AARD).

T (K)	P (bar)	D_{11}^{exp} ($10^{-9} \text{ m}^2 \text{ s}^{-1}$)	D_{11}^{MD} ($10^{-9} \text{ m}^2 \text{ s}^{-1}$)	RD (%)
298.15	1	1.05	1.01	−3.81
308.15	1	1.30	1.29	−0.77
318.15	1	1.68	1.61	−4.17
328.15	1	2.06	2.00	−2.91
333.15	1	2.37	2.23	−5.91

ARD = −3.51%
AARD = 3.51%

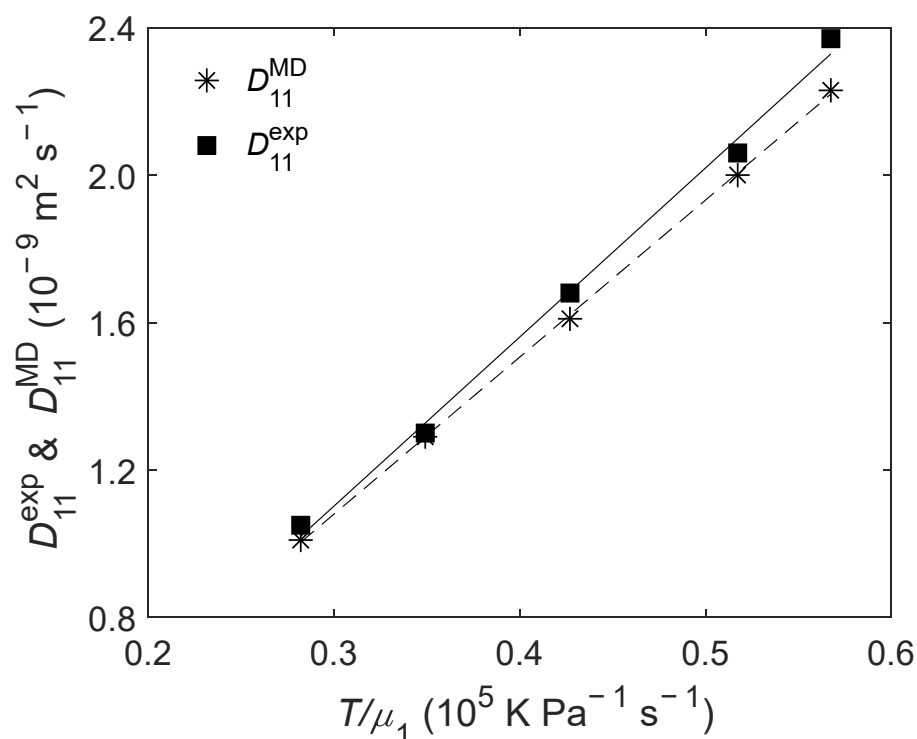


Figure 4. Experimental (D_{11}^{exp} , ■) and computed (D_{11}^{MD} , *) self-diffusion coefficients of ethanol versus Stokes–Einstein abscissae. The viscosity values were estimated by the Mamedov equation, as proposed by Cano-Gómez et al. [44].

2.4. Influence of the Oxygen's Energy Parameter

The influence of the Lennard-Jones energy parameter of ethanol's oxygen (ϵ_{OH}) in the D_{11}^{MD} of ethanol and D_{12}^{MD} of quercetin and benzene in ethanol was also analyzed. It was found that increasing by 20% the value of ϵ_{OH} (i.e., the value was made equal to the one in the TraPPE-UA force field [26]) for calculations of D_{11}^{MD} of ethanol at 298.15 K and 1 bar, with $\sigma_{\text{OH}} = 0.306$ nm, originated a minor improvement of the diffusivity (RD changed from −3.81% to 1.90%) without negatively affecting the density (RD was barely the same), suggesting that additional improvements can be made by fine tuning the value of ϵ_{OH} . In the case of the original $\sigma_{\text{OH}} = 0.312$ nm, the increase by 20% of ϵ_{OH} led to an increase of RD from 33.33% to 38.10%, while a decrease by 20% of ϵ_{OH} decreased RD from 33.33% to 25.71%, which suggests that fine tuning of the energy scale with the original radius value will hardly lead to a significant improvement in the D_{11}^{MD} of ethanol.

As it happened with the D_{11}^{MD} of ethanol, a systematic shift of the RD to more positive values was found for the protic compound quercetin when the value of ϵ_{OH} was increased by 20%. For example, when employing $\sigma_{OH} = 0.306$ nm, the RD for the calculated diffusivity, at 1 bar and 303.15 K, changed from -6.30% to 1.55% , while the value at 1 bar and 323.15 K changed from 3.13% to -7.10% . However, such systematic variation was not found in the case of the non-polar benzene molecule. In fact, when employing $\sigma_{OH} = 0.306$ nm, the RD for the calculated diffusivity, at 1 bar and 313.15 K, changed from -18.86% to -19.30% .

The results above suggest that it may be possible to slightly decrease the RD values between calculated and experimental results upon tuning the ϵ_{OH} parameter but also that two different σ_{OH} values are needed for protic and non-polar solutes, i.e., it will be difficult to find a unique solution for all kinds of solutes. Hence, a new σ_{OH} of ethanol's oxygen atom is proposed while fixing the energy parameter (ϵ_{OH}).

2.5. Equilibrium Properties of Ethanol

Typically, two properties used for the force-field calibration and validation are the enthalpy of vaporization (ΔH_{vap}) and density (ρ). Contrary to what was verified in the case of diffusivities, when the original value $\sigma_{OH} = 0.312$ nm is used for the calculation of ΔH_{vap} , the computed value (42.0 kJ mol⁻¹) compares well with the experimental result (42.3 ± 0.4 kJ mol⁻¹ [45]), with RD = -0.71% . When the reparametrized value ($\sigma_{OH} = 0.306$ nm) is used, the computed value of ΔH_{vap} increases to 44.8 kJ mol⁻¹, which is 5.91% higher than the one computed with $\sigma_{OH} = 0.312$ nm. This difference is mainly due to the computed potential energy of the liquid phase (U_{liquid}) being around 13% higher when using $\sigma_{OH} = 0.312$ nm.

As for density, the values computed with $\sigma_{OH} = 0.306$ nm are always higher than the ones computed with $\sigma_{OH} = 0.312$ nm. This trend was already expected since, as stated before, a smaller σ_{OH} value means the molecules may be closer to each other; hence, density increases. As for the density values computed with $\sigma_{OH} = 0.306$ nm, RD values ranged between 1.59% and 2.58% for 298.15 K $\leq T \leq 333.15$ K at 1 bar. At a higher-pressure of 300 bar, the density values, computed at 308.15 K and 333.15 K, were also higher than the experimental ones with RD of 2.77% and 1.41% , respectively. Globally, this translates into an AARD = 2.12% and ARD of same value, which are both higher than the results obtained when using the original σ_{OH} value (AARD = 0.46% and ARD = 0.34%). These results are summarized in Table 4, and comparison between these density values and the ones obtained with $\sigma_{OH} = 0.312$ nm can be found in Table S4.

Table 4. Ethanol's experimental (ρ^{exp}) and computed (ρ^{MD}) density and respective relative deviation (RD). The computer simulations used $\sigma_{OH} = 0.306$ nm for ethanol.

<i>T</i> (K)	<i>P</i> (bar)	ρ^{exp} (kg m ⁻³)	ρ^{MD} (kg m ⁻³)	RD (%)
298.15	1	786	806	2.54
308.15	1	776	796	2.58
308.15	300	795	817	2.77
318.15	1	767	785	2.08
328.15	1	759	773	1.84
333.15	1	754	768	1.59
333.15	300	782	793	1.41

ARD = 2.12%
AARD = 2.12%

3. Materials and Methods

3.1. Database

The database compiled for evaluation and optimization of the ethanol's oxygen diameter (σ_{OH}) is summarized in Table 5 for solute/ethanol or pure ethanol systems. Six polar-solute systems (namely, quercetin, gallic acid, ibuprofen, butan-1-ol, propanone,

and butanal, with structural formulas in Figure 5) and two systems comprising non-polar solutes (benzene and propane, also shown in Figure 5) were considered. The first two polar-solutes (i.e., quercetin and gallic acid) were used for optimization of the σ_{OH} value, while the second pair of polar solutes (i.e., ibuprofen and butan-1-ol) was selected for validation of the new proposed value. The remaining polar (i.e., propanone and butanal) alongside the non-polar solutes were chosen to investigate the initial hypothesis that OPLS-AA overestimates D_{12} of protic solutes. Ethanol properties, such as D_{11} , density (ρ), and enthalpy of vaporization (ΔH_{vap}) were also included.

Table 5. Experimental properties studied for binary (ethanol/solute) or unary (ethanol) systems, number of data points (NDP), temperature (T) range, pressure (P) range, and data sources.

System	Property	NDP	T (K)	P (bar)	Source
EtOH/quercetin	D_{12}	4	303.15–323.15	1–150	[46]
EtOH/gallic acid	D_{12}	3	303.15–333.15	1	[5]
EtOH/ibuprofen	D_{12}	8	298.15–333.15	1–300	[4]
EtOH/butan-1-ol	D_{12}	2	298.15–333.15	1	[47]
EtOH/propanone	D_{12}	2	298.15–333.15	1	[48]
EtOH/butanal	D_{12}	2	298.15–333.15	1	[48]
EtOH/benzene	D_{12}	1	313.15	1	[47,49]
EtOH/propane	D_{12}	1	323.15	103	[50]
EtOH	D_{11}	5	298.15–333.15	1	[51–58]
EtOH	ρ	8	298.15–333.15	1–300	[59–62]
EtOH	ΔH_{vap}	1	298.15	1	[45]

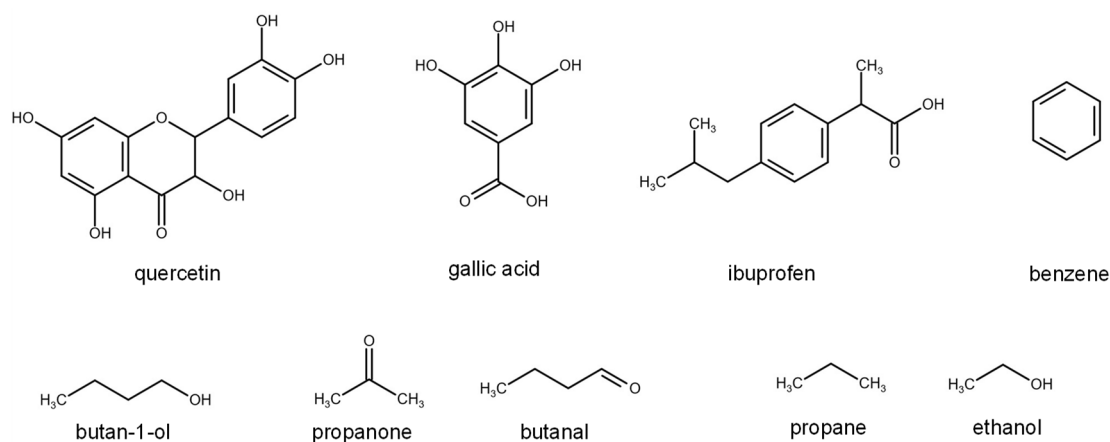


Figure 5. Structural formulas of the compounds studied in this work.

All the results calculated in this work were evaluated in terms of relative deviations (RD), average relative deviations (ARD), and average absolute relative deviations (AARD) calculated by:

$$RD(\%) = 100 \frac{X^{MD} - X^{exp}}{X^{exp}} \quad (1)$$

$$ARD(\%) = \frac{100}{NDP} \sum_{i=1}^{NDP} \left(\frac{X^{MD} - X^{exp}}{X^{exp}} \right)_i \quad (2)$$

$$AARD(\%) = \frac{100}{NDP} \sum_{i=1}^{NDP} \left| \frac{X^{MD} - X^{exp}}{X^{exp}} \right|_i \quad (3)$$

in which X is the property under study, NDP is the number of data points, and the superscripts MD and exp represent the computed and experimental property, respectively.

3.2. Molecular Dynamics Simulation Procedure

The classical MD simulations were carried out with the GROMACS 2019 code [63–65], using cubic boxes with 3500 molecules of ethanol and 4–20 molecules of the solute, corresponding to a mass fraction in the range between 0.5% and 1%. The precise number of solute molecules used for each system can be found in Supplementary Materials (Table S5).

The potential parameters used in this work for the different compounds are supplied in a separate zip file in a format (.itp) that is compatible with the GROMACS code. The equations used for calculation of the interactions and the topologies of the solute molecules can be found in Supplementary Materials (Equations (S1)–(S8)). For each temperature/pressure condition, the simulations were carried out using a published procedure by Zêzere et al. [20], with longer simulation times, based on the computational recipe proposed by Barrera and Jorge [23]. Each simulation was initialized by a steepest-descent minimization run, followed by a 100 ps simulation using the canonical ensemble (NVT) with initial velocities generated according to the Maxwell–Boltzmann distribution; next, a 100 ps run in the isothermal–isobaric ensemble (NPT) was carried out using the Berendsen coupling scheme [66]; finally, the simulation continued in the NPT ensemble up to a few nanoseconds (see below) with a time step of 0.001 ps. The last phase of the simulation was carried out using the leap-frog algorithm [67], with the box temperature and pressure being kept constant by using the V-rescale thermostat [68] and the Parrinello–Rahman barostat [69], respectively. The choice for the NPT ensemble was to certify that the simulations were performed at the same pressure and temperature conditions used to measure experimental data. Nevertheless, in previous work, it was found that diffusivities calculated from NVT and NPT simulations are very similar, with the main difference being the average pressure of the simulation [20]. Additionally, the LINCS algorithm was used to constrain the bond lengths, and a cut-off distance of 1.4 nm was adopted, as tested in a previous work [20], for both van der Waals and Coulomb interactions. The Particle–Mesh Ewald (PME) [70] summation was selected for the long-range electrostatic interactions. The simulation was carried out using the standard periodic boundary conditions, applying long-range dispersion corrections for energy and pressure. The compressibility values were taken from the literature [71] or estimated using published correlations [59]. As for the duration of the simulations, these were adjusted according to the desired property, as indicated in Sections 3.3 and 3.4.

3.3. Self-Diffusion and Binary Diffusion Coefficients

The diffusion coefficients (D_{11} or D_{12}) were calculated by the Einstein relation of the mean square displacement (MSD) of the random motion of a molecule [72]:

$$D_{11} \text{ or } D_{12} = \lim_{t \rightarrow \infty} \frac{\langle [r(t_0 + t) - r(t_0)]^2 \rangle}{6t} \quad (4)$$

in which t_0 is the time origin, t is the time elapsed from t_0 , and r is the molecule/atom position. The average, represented by the angled brackets, was calculated using all molecules in the simulation and all time origins. Once the MSD as a function of time was known, a simple linear least-squares regression was performed between 50 and 100 ps, as shown previously, to yield accurate results [20].

For the D_{12} calculations, the final NPT ensemble was carried out during 40 ns of which the first 20 ns were discarded to assure proper equilibration of the dynamics [20]. The final D_{12} value was obtained from averaging the D_{12} results of three independent simulation replicas.

As for D_{11} calculations, the simulations were carried out with the setup previously described, with 10 ns of equilibration and 15 ns of production, and only one simulation was considered for the final D_{11} value. Typically, the computed D_{11} values are affected by the finite size of the simulation box. Hence, a correction should be introduced to overcome this limitation which, according to Yeh and Hummer [73], can be conducted by performing a

linear regression between $D_{11}^{\text{MD},L}$, the self-diffusion coefficient computed from a simulation box with finite length L , and $1/L$. Accordingly:

$$D_{11}^{\text{MD},L} = m \times \frac{1}{L} + D_{11}^{\text{MD},\infty} \quad (5)$$

where $D_{11}^{\text{MD},\infty}$ is the self-diffusion coefficient computed from the simulation box with infinite length (y -intercept at $1/L = 0$), and m is the slope. Alternatively, a hydrodynamic correction can be directly applied [73]:

$$D^{\text{YH}}(T, \mu_1, L) = \frac{\xi k_B T}{6\pi\mu_1 L} \quad (6)$$

$$D_{11}^{\text{MD},\infty} = D_{11}^{\text{MD},L} + D^{\text{YH}}(T, \mu_1, L) \quad (7)$$

in which $D^{\text{YH}}(T, \mu_1, L)$ is the Yeh and Hummer hydrodynamic correction of $D_{11}^{\text{MD},L}$, k_B is the Boltzmann constant ($1.380649 \times 10^{-23} \text{ m}^2 \text{ kg s}^{-2} \text{ K}^{-1}$), ξ is a dimensional constant of value 2.837297, and μ_1 the viscosity. This second approach was adopted in this work since it is computationally cheaper, and the $D_{11}^{\text{MD},\infty}$ results are equivalent to those obtained by the linear regression method, as depicted in Figure S1 (see Supplementary Materials). A total of 1500 ethanol molecules were used per simulation at each condition.

3.4. Calculation of Equilibrium Properties

3.4.1. Enthalpy of Vaporization

The enthalpy of vaporization was computed by:

$$\Delta H_{\text{vap}} = U_{\text{gas}} - U_{\text{liquid}} + R_g T \quad (8)$$

in which U_{gas} is the potential energy of the vapor phase, U_{liquid} the potential energy of the liquid phase, and R_g the ideal gas constant ($R_g = 8.314 \text{ J K}^{-1} \text{ mol}^{-1}$). To calculate U_{liquid} , we used the last 15 ns of the simulation used to compute D_{11} . The Barrera and Jorge [23] procedure was used to calculate U_{gas} , with one molecule being placed inside a cubic box ($15 \text{ nm} \times 15 \text{ nm} \times 15 \text{ nm}$), with no boundary conditions and all cutoff radii set to 0. The simulation was carried out in NVT using the leap-frog stochastic dynamics integrator, which adds a friction and a noise term to Newton's equation of motion [74]. The run was carried out for 50 ns, and the first 10 ns of the simulation were discarded.

3.4.2. Density

The densities of pure ethanol systems were calculated from the last 15 ns of the trajectories. For conditions for which no D_{11} was computed, the simulations were carried out with the setup used for D_{11} calculation.

4. Conclusions

The OPLS-AA force field was used in the calculation of tracer diffusion coefficients (D_{12}) of solutes in ethanol and of self-diffusion coefficients (D_{11}) of ethanol from molecular dynamics simulations carried out at different temperature and pressure conditions. It was found that when the oxygen atom of ethanol considers the original OPLS-AA diameter, it yields high deviations of D_{11} of ethanol and of D_{12} of protic solutes in ethanol.

In order to correct such deviations, the diameter of the oxygen atom (σ_{OH}) of ethanol was reoptimized by targeting D_{12} of quercetin and of gallic acid (both protic solutes) in liquid ethanol, at $303.15 \text{ K} \leq T \leq 323.15 \text{ K}$ and P up to 150 bar, and $303.15 \text{ K} \leq T \leq 333.15 \text{ K}$ and $P = 1 \text{ bar}$, respectively. With the new optimized value, i.e., $\sigma_{\text{OH}} = 0.306 \text{ nm}$, the comparison with the experiment was substantially improved, with an average absolute relative deviation (AARD) of 3.71% and average relative deviation (ARD) of -0.04% for quercetin and AARD = 4.59% and ARD = 1.05% for gallic acid.

Significant improvements were also found for the computed D_{12} of ibuprofen in liquid ethanol at $298.15 \text{ K} \leq T \leq 333.15 \text{ K}$ and P up to 300 bar, with AARD = 1.55% and ARD = 0.70%, and for butan-1-ol at $298.15 \text{ K} \leq T \leq 333.15 \text{ K}$ and $P = 1$ bar, with AARD = 4.81% and ARD = 4.05%. A mixed behavior was observed for propanone and butanal for which the results improved at $T = 333.15 \text{ K}$ but significantly deteriorated at $T = 303.15 \text{ K}$. However, in the case of non-polar solutes such as propane or benzene, the performance worsened with the new value at all the tested conditions. Regarding the D_{11} of ethanol, the results vastly improved, having achieved AARD and ARD values of 3.51% and -3.51% , respectively, at the tested conditions.

In all the test systems, when computing either D_{12} or D_{11} , the expected trends with T , P , and Stokes–Einstein abscissae were always conserved.

Finally, the influence of the new value was evaluated in both enthalpy of vaporization (ΔH_{vap}) and density of ethanol, achieving slightly worse results in both cases with RD = 5.91% for ΔH_{vap} and AARD = 2.12% and ARD of same value for density. Hence, the value of $\sigma_{\text{OH}} = 0.306 \text{ nm}$ is recommended only for the calculations of D_{12} of protic solutes containing OH in pure liquid ethanol and D_{11} estimation.

Supplementary Materials: The supporting information can be downloaded at: <https://www.mdpi.com/article/10.3390/ijms24087316/s1>.

Author Contributions: B.Z.: Methodology, investigation, writing—original draft; T.V.B.F.: investigation, writing—original draft; I.P.: writing—review and editing, formal analysis; M.M.Q.S.: supervision, formal analysis; C.M.S.: supervision, conceptualization, resources, writing—review and editing, funding acquisition, formal analysis; J.R.B.G.: supervision, resources, conceptualization, formal analysis, writing—review and editing. All authors have read and agreed to the published version of the manuscript.

Funding: This work was developed within the scope of the project CICECO-Aveiro Institute of Materials, UIDB/50011/2020, UIDP/50011/2020, and LA/P/0006/2020, financed by national funds through the FCT/MEC (PIDDAC) and also through project GCORK, POCI-01-0247-FEDER-070302. Bruno Zêzere thanks FCT for the PhD grant SFRH/BD/137751/2018.

Institutional Review Board Statement: Not applicable.

Informed Consent Statement: Not applicable.

Data Availability Statement: The raw/processed data required to reproduce the above findings cannot be shared at this time due to technical/time limitations.

Conflicts of Interest: The authors declare no conflict of interest.

References

1. Taylor, R.; Krishna, R. Multicomponent Mass Transfer. In *Wiley Series in Chemical Engineering*; John Wiley & Sons, Inc.: New York, NY, USA, 1993.
2. Oliveira, E.L.G.; Silvestre, A.J.D.; Silva, C.M. Review of kinetic models for supercritical fluid extraction. *Chem. Eng. Res. Des.* **2011**, *89*, 1104–1117. [[CrossRef](#)]
3. Zêzere, B.; Portugal, I.; Gomes, J.R.B.; Silva, C.M. Modeling Tracer Diffusion Coefficients of Any Type of Solutes in Polar and Non-Polar Dense Solvents. *Materials* **2022**, *15*, 6416. [[CrossRef](#)] [[PubMed](#)]
4. Kong, C.Y.; Sugiura, K.; Natsume, S.; Sakabe, J.; Funazukuri, T.; Miyake, K.; Okajima, I.; Badhulika, S.; Sako, T. Measurements and correlation of diffusion coefficients of ibuprofen in both liquid and supercritical fluids. *J. Supercrit. Fluids* **2020**, *159*, 104776. [[CrossRef](#)]
5. Leite, J.; Magalhães, A.L.; Valente, A.A.; Silva, C.M. Measurement and modelling of tracer diffusivities of gallic acid in liquid ethanol and in supercritical CO₂ modified with ethanol. *J. Supercrit. Fluids* **2018**, *131*, 130–139. [[CrossRef](#)]
6. Cai, G.; Katsumata, W.; Okajima, I.; Sako, T.; Funazukuri, T.; Kong, C.Y. Determination of diffusivities of triolein in pressurized liquids and in supercritical CO₂. *J. Mol. Liq.* **2022**, *354*, 118860. [[CrossRef](#)]
7. Taylor, G. Dispersion of soluble matter in solvent flowing slowly through a tube. *Proc. R. Soc. A Math. Phys. Eng. Sci.* **1953**, *219*, 186–203. [[CrossRef](#)]
8. Taylor, G. Diffusion and mass transport in tubes. *Proc. Phys. Soc. Sect. B* **1954**, *67*, 857–869. [[CrossRef](#)]
9. Taylor, G. The dispersion of matter in turbulent flow through a pipe. *Proc. R. Soc. A Math. Phys. Eng. Sci.* **1954**, *223*, 446–468. [[CrossRef](#)]

10. Aris, R. On the dispersion of a solute by diffusion, convection and exchange between phases. *Proc. R. Soc. A Math. Phys. Eng. Sci.* **1959**, *252*, 538–550. [[CrossRef](#)]
11. Wilke, C.R.; Chang, P. Correlation of diffusion coefficients in dilute solutions. *AIChE J.* **1955**, *1*, 264–270. [[CrossRef](#)]
12. Poling, B.E.; Prausnitz, J.M.; O'Connell, J.P. *The Properties of Gases and Liquids*, 5th ed.; Company, M.-H.B., Ed.; The McGraw-Hill Companies, Inc.: New York, NY, USA, 2001; ISBN 0071499997.
13. Aniceto, J.P.S.; Zêzere, B.; Silva, C.M. Predictive Models for the Binary Diffusion Coefficient at Infinite Dilution in Polar and Nonpolar Fluids. *Materials* **2021**, *14*, 542. [[CrossRef](#)] [[PubMed](#)]
14. Silva, C.M.; Liu, H. Modelling of Transport Properties of Hard Sphere Fluids and Related Systems, and its Applications. In *Theory and Simulation of Hard-Sphere Fluids and Related Systems*; Mulero, A., Ed.; Springer: Berlin/Heidelberg, Germany, 2008; Volume 753, pp. 383–492. ISBN 978-3-540-78766-2.
15. Dymond, J.H. Corrected Enskog theory and the transport coefficients of liquids. *J. Chem. Phys.* **1974**, *60*, 969–973. [[CrossRef](#)]
16. Dymond, J.H.; Bich, E.; Vogel, E.; Wakeham, W.A.; Vesovic, V.; Assael, M.J. Dense fluids. In *Transport Properties of Fluids—Their Correlation, Prediction and Estimation*; Millat, J., Dymond, J.H., Nieto de Castro, C.A., Eds.; Cambridge University Press: Cambridge, UK, 1996; pp. 66–112.
17. Aniceto, J.P.S.; Zêzere, B.; Silva, C.M. Machine learning models for the prediction of diffusivities in supercritical CO₂ systems. *J. Mol. Liq.* **2021**, *326*, 115281. [[CrossRef](#)]
18. Allers, J.P.; Priest, C.W.; Greathouse, J.A.; Alam, T.M. Using Computationally-Determined Properties for Machine Learning Prediction of Self-Diffusion Coefficients in Pure Liquids. *J. Phys. Chem. B* **2021**, *125*, 12990–13002. [[CrossRef](#)] [[PubMed](#)]
19. Allers, J.P.; Keth, J.; Alam, T.M. Prediction of Self-Diffusion in Binary Fluid Mixtures Using Artificial Neural Networks. *J. Phys. Chem. B* **2022**, *126*, 4555–4564. [[CrossRef](#)] [[PubMed](#)]
20. Zêzere, B.; Portugal, I.; Silva, C.M.; Gomes, J.R.B. Diffusivities of ketones and aldehydes in liquid ethanol by molecular dynamics simulations. *J. Mol. Liq.* **2023**, *371*, 121068. [[CrossRef](#)]
21. Vaz, R.V.; Gomes, J.R.B.; Silva, C.M. Molecular dynamics simulation of diffusion coefficients and structural properties of ketones in supercritical CO₂ at infinite dilution. *J. Supercrit. Fluids* **2016**, *107*, 630–638. [[CrossRef](#)]
22. Baba, H.; Urano, R.; Nagai, T.; Okazaki, S. Prediction of self-diffusion coefficients of chemically diverse pure liquids by all-atom molecular dynamics simulations. *J. Comput. Chem.* **2022**, *43*, 1892–1900. [[CrossRef](#)]
23. Barrera, M.C.; Jorge, M. A Polarization-Consistent Model for Alcohols to Predict Solvation Free Energies. *J. Chem. Inf. Model.* **2020**, *60*, 1352–1367. [[CrossRef](#)]
24. Bordonhos, M.; Galvão, T.L.P.; Gomes, J.R.B.; Gouveia, J.D.; Jorge, M.; Lourenço, M.A.O.; Pereira, J.M.; Pérez-Sánchez, G.; Pinto, M.L.; Silva, C.M.; et al. Multiscale Computational Approaches toward the Understanding of Materials. *Adv. Theory Simul.* **2022**, *2200628*. [[CrossRef](#)]
25. Marrink, S.J.; de Vries, A.H.; Mark, A.E. Coarse Grained Model for Semiquantitative Lipid Simulations. *J. Phys. Chem. B* **2004**, *108*, 750–760. [[CrossRef](#)]
26. Eggimann, B.L.; Sun, Y.; DeJaco, R.F.; Singh, R.; Ahsan, M.; Josephson, T.R.; Siepmann, J.I. Assessing the Quality of Molecular Simulations for Vapor–Liquid Equilibria: An Analysis of the TraPPE Database. *J. Chem. Eng. Data* **2020**, *65*, 1330–1344. [[CrossRef](#)]
27. Wang, J.; Wang, W.; Kollman, P.A.; Case, D.A. Automatic atom type and bond type perception in molecular mechanical calculations. *J. Mol. Graph. Model.* **2006**, *25*, 247–260. [[CrossRef](#)] [[PubMed](#)]
28. Jorgensen, W.L.; Maxwell, D.S.; Tirado-Rives, J. Development and Testing of the OPLS All-Atom Force Field on Conformational Energetics and Properties of Organic Liquids. *J. Am. Chem. Soc.* **1996**, *118*, 11225–11236. [[CrossRef](#)]
29. Siu, S.W.I.; Pluhackova, K.; Böckmann, R.A. Optimization of the OPLS-AA Force Field for Long Hydrocarbons. *J. Chem. Theory Comput.* **2012**, *8*, 1459–1470. [[CrossRef](#)]
30. Pluhackova, K.; Morhenn, H.; Lautner, L.; Lohstroh, W.; Nemkovski, K.S.; Unruh, T.; Böckmann, R.A. Extension of the LOPLS-AA Force Field for Alcohols, Esters, and Monoolein Bilayers and its Validation by Neutron Scattering Experiments. *J. Phys. Chem. B* **2015**, *119*, 15287–15299. [[CrossRef](#)]
31. Robertson, M.J.; Tirado-Rives, J.; Jorgensen, W.L. Improved Peptide and Protein Torsional Energetics with the OPLS-AA Force Field. *J. Chem. Theory Comput.* **2015**, *11*, 3499–3509. [[CrossRef](#)]
32. Lu, C.; Wu, C.; Ghoreishi, D.; Chen, W.; Wang, L.; Damm, W.; Ross, G.A.; Dahlgren, M.K.; Russell, E.; Von Bargen, C.D.; et al. OPLS4: Improving Force Field Accuracy on Challenging Regimes of Chemical Space. *J. Chem. Theory Comput.* **2021**, *17*, 4291–4300. [[CrossRef](#)]
33. Zangi, R. Refinement of the OPLSAA Force-Field for Liquid Alcohols. *ACS Omega* **2018**, *3*, 18089–18099. [[CrossRef](#)]
34. Kulschewski, T.; Pleiss, J. A molecular dynamics study of liquid aliphatic alcohols: Simulation of density and self-diffusion coefficient using a modified OPLS force field. *Mol. Simul.* **2013**, *39*, 754–767. [[CrossRef](#)]
35. Zhang, X.; Wang, Y.; Yao, J.; Li, H.; Mochizuki, K. A tiny charge-scaling in the OPLS-AA + L-OPLS force field delivers the realistic dynamics and structure of liquid primary alcohols. *J. Comput. Chem.* **2022**, *43*, 421–430. [[CrossRef](#)] [[PubMed](#)]
36. Petravic, J.; Delhommelle, J. Influence of temperature, pressure and internal degrees of freedom on hydrogen bonding and diffusion in liquid ethanol. *Chem. Phys.* **2003**, *286*, 303–314. [[CrossRef](#)]
37. Cardona, J.; Fartaria, R.; Sweatman, M.B.; Lue, L. Molecular dynamics simulations for the prediction of the dielectric spectra of alcohols, glycols and monoethanolamine. *Mol. Simul.* **2016**, *42*, 370–390. [[CrossRef](#)]

38. Schnabel, T.; Vrabc, J.; Hasse, H. Henry's law constants of methane, nitrogen, oxygen and carbon dioxide in ethanol from 273 to 498 K: Prediction from molecular simulation. *Fluid Phase Equilib.* **2005**, *233*, 134–143. [CrossRef]
39. Guevara-Carrion, G.; Nieto-Draghi, C.; Vrabc, J.; Hasse, H. Prediction of Transport Properties by Molecular Simulation: Methanol and Ethanol and Their Mixture. *J. Phys. Chem. B* **2008**, *112*, 16664–16674. [CrossRef]
40. Hirschfelder, J.O.; Curtiss, C.F.; Bird, R.B. *The Molecular Theory of Gases and Liquids*; John Wiley & Sons Inc: New York, NY, USA, 1964; ISBN 9780471400653.
41. Liu, H.; Silva, C.M.; Macedo, E.A. Unified approach to the self-diffusion coefficients of dense fluids over wide ranges of temperature and pressure—Hard-sphere, square-well, Lennard-Jones and real substances. *Chem. Eng. Sci.* **1998**, *53*, 2403–2422. [CrossRef]
42. Silva, C.M.; Liu, H.; Macedo, E.A. Models for self-diffusion coefficients of dense fluids, including hydrogen-bonding substances. *Chem. Eng. Sci.* **1998**, *53*, 2423–2429. [CrossRef]
43. Liu, H.; Silva, C.M.; Macedo, E.A. Generalised free-volume theory for transport properties and new trends about the relationship between free volume and equations of state. *Fluid Phase Equilib.* **2002**, *202*, 89–107. [CrossRef]
44. Cano-Gómez, J.J.; Iglesias-Silva, G.A.; Ramos-Estrada, M. Correlations for the prediction of the density and viscosity of 1-alcohols at high pressures. *Fluid Phase Equilib.* **2015**, *404*, 109–117. [CrossRef]
45. National Institute of Standards and Technology NIST Chemistry WebBook—Ethanol. Available online: <https://webbook.nist.gov/cgi/cbook.cgi?ID=C64175&Mask=4> (accessed on 11 December 2022).
46. Zêzere, B.; Iglésias, J.; Portugal, I.; Gomes, J.R.B.; Silva, C.M. Diffusion of quercetin in compressed liquid ethyl acetate and ethanol. *J. Mol. Liq.* **2020**, *324*, 114714. [CrossRef]
47. Tominaga, T.; Matsumoto, S. Diffusion of polar and nonpolar molecules in water and ethanol. *Bull. Chem. Soc. Jpn.* **1990**, *63*, 533–537. [CrossRef]
48. Zêzere, B.; Buchgeister, S.; Faria, S.; Portugal, I.; Gomes, J.R.B.; Silva, C.M. Diffusivities of linear unsaturated ketones and aldehydes in compressed liquid ethanol. *J. Mol. Liq.* **2022**, *367*, 120480. [CrossRef]
49. Sun, C.K.J.; Chen, S.H. Tracer diffusion in dense ethanol: A generalized correlation for nonpolar and hydrogen-bonded solvents. *AIChE J.* **1986**, *32*, 1367–1371. [CrossRef]
50. Cooper, E. *Diffusion Coefficients at Infinite Dilution in Alcohol Solvents at Temperatures to 348 K and Pressures to 17 MPa*; University of Ottawa: Ottawa, ON, Canada, 1992.
51. Meckl, S.; Zeidler, M.D. Self-diffusion measurements of ethanol and propanol. *Mol. Phys.* **1988**, *63*, 85–95. [CrossRef]
52. Hardt, A.P.; Anderson, D.K.; Rathbun, R.; Mar, B.W.; Babb, A.L. Self-Diffusion in Liquids. II. Comparison between Mutual and Self-Diffusion Coefficients. *J. Phys. Chem.* **1959**, *63*, 2059–2061. [CrossRef]
53. Rathbun, R.E.; Babb, A.L. Self-diffusion in liquids. III. Temperature dependence in pure liquids. *J. Phys. Chem.* **1961**, *65*, 1072–1074. [CrossRef]
54. Hurler, R.L.; Eastal, A.J.; Woolf, L.A. Self-diffusion in monohydric alcohols under pressure. Methanol, methan(2H)ol and ethanol. *J. Chem. Soc. Faraday Trans. 1 Phys. Chem. Condens. Phases* **1985**, *81*, 769. [CrossRef]
55. Johnson, P.A.; Babb, A.L. Self-diffusion in Liquids. 1. Concentration Dependence in Ideal and Non-ideal Binary Solutions. *J. Phys. Chem.* **1956**, *60*, 14–19. [CrossRef]
56. Partington, J.R.; Hudson, R.F.; Bagnall, K.W. Self-diffusion of Aliphatic Alcohols. *Nature* **1952**, *169*, 583–584. [CrossRef]
57. Graupner, K.; Winter, E.R.S. 201. Some measurements of the self-diffusion coefficients of liquids. *J. Chem. Soc.* **1952**, 1145–1150. [CrossRef]
58. Holz, M.; Weingartner, H. Calibration in accurate spin-echo self-diffusion measurements using ¹H and less-common nuclei. *J. Magn. Reson.* **1991**, *92*, 115–125. [CrossRef]
59. Zeberg-Mikkelsen, C.K.; Lugo, L.; Fernández, J. Density measurements under pressure for the binary system (ethanol+methylcyclohexane). *J. Chem. Thermodyn.* **2005**, *37*, 1294–1304. [CrossRef]
60. Mokhtarani, B.; Sharifi, A.; Mortaheb, H.R.; Mirzaei, M.; Mafi, M.; Sadeghian, F. Density and viscosity of 1-butyl-3-methylimidazolium nitrate with ethanol, 1-propanol, or 1-butanol at several temperatures. *J. Chem. Thermodyn.* **2009**, *41*, 1432–1438. [CrossRef]
61. Zhu, T.; Gong, H.; Dong, M. Density and viscosity of CO₂ + ethanol binary systems measured by a capillary viscometer from 308.15 to 338.15 K and 15 to 45 MPa. *J. Chem. Eng. Data* **2020**, *65*, 3820–3833. [CrossRef]
62. Watson, G.; Zeberg-Mikkelsen, C.K.; Baylaucq, A.; Boned, C. High-Pressure Density Measurements for the Binary System Ethanol + Heptane. *J. Chem. Eng. Data* **2006**, *51*, 112–118. [CrossRef]
63. Lindahl, E.; Abraham, M.J.; Hess, B.; van der Spoel, D. *GROMACS 2019.3 Manual*; 2019. [CrossRef]
64. Lindahl, E.; Abraham, M.J.; Hess, B.; Van Der Spoel, D. *GROMACS 2019.3 Source Code* 2019. [CrossRef]
65. Abraham, M.J.; Murtola, T.; Schulz, R.; Páll, S.; Smith, J.C.; Hess, B.; Lindahl, E. GROMACS: High performance molecular simulations through multi-level parallelism from laptops to supercomputers. *SoftwareX* **2015**, *1–2*, 19–25. [CrossRef]
66. Berendsen, H.J.C.; Postma, J.P.M.; van Gunsteren, W.F.; DiNola, A.; Haak, J.R. Molecular dynamics with coupling to an external bath. *J. Chem. Phys.* **1984**, *81*, 3684–3690. [CrossRef]
67. Hockney, R.W.; Goel, S.P.; Eastwood, J.W. Quiet high-resolution computer models of a plasma. *J. Comput. Phys.* **1974**, *14*, 148–158. [CrossRef]
68. Bussi, G.; Donadio, D.; Parrinello, M. Canonical sampling through velocity rescaling. *J. Chem. Phys.* **2007**, *126*, 014101. [CrossRef]

69. Parrinello, M.; Rahman, A. Polymorphic transitions in single crystals: A new molecular dynamics method. *J. Appl. Phys.* **1981**, *52*, 7182–7190. [[CrossRef](#)]
70. Essmann, U.; Perera, L.; Berkowitz, M.L.; Darden, T.; Lee, H.; Pedersen, L.G. A smooth particle mesh Ewald method. *J. Chem. Phys.* **1995**, *103*, 8577–8593. [[CrossRef](#)]
71. DDBST GmbH Compressibility (Isothermal) of Ethanol. Available online: http://www.ddbst.com/en/EED/PCP/CMPT_C11.php (accessed on 18 March 2022).
72. Hoheisel, C. Computer Calculation. In *Transport Properties of Fluids. Their Correlation, Prediction and Estimation*; Millat, J., Dymond, J.H., Nieto de Castro, C.A., Eds.; Cambridge University Press: Cambridge, UK, 1996.
73. Yeh, I.-C.; Hummer, G. System-Size Dependence of Diffusion Coefficients and Viscosities from Molecular Dynamics Simulations with Periodic Boundary Conditions. *J. Phys. Chem. B* **2004**, *108*, 15873–15879. [[CrossRef](#)]
74. Caleman, C.; van Maaren, P.J.; Hong, M.; Hub, J.S.; Costa, L.T.; van der Spoel, D. Force Field Benchmark of Organic Liquids: Density, Enthalpy of Vaporization, Heat Capacities, Surface Tension, Isothermal Compressibility, Volumetric Expansion Coefficient, and Dielectric Constant. *J. Chem. Theory Comput.* **2012**, *8*, 61–74. [[CrossRef](#)] [[PubMed](#)]

Disclaimer/Publisher's Note: The statements, opinions and data contained in all publications are solely those of the individual author(s) and contributor(s) and not of MDPI and/or the editor(s). MDPI and/or the editor(s) disclaim responsibility for any injury to people or property resulting from any ideas, methods, instructions or products referred to in the content.